AIAA JOURNAL
Vol. 39, No. 5, May 2001

# Dynamics of an Inflatable Structure in Vacuum and Ambient Conditions

Kara N. Slade*
*Duke University, Durham, North Carolina 27708-0300*
and
Michael L. Tinker,† John O. Lassiter,‡ and Robert Engberg§
*NASA Marshall Space Flight Center, Huntsville, Alabama 35812*

**In the dynamic modal testing of extremely lightweight inflatable structures, the results may vary dramatically according to the presence of either thermal vacuum or ambient atmospheric conditions. Unique aspects of modal testing techniques for an inflatable solar concentrator are identified, including the use of a noncontacting laser vibrometer measurement system. For the thermal vacuum environment, mode shapes and frequency response functions are compared for three different test article inflation pressures at room temperature. Modes that persist through all inflation pressure regimes are identified, as are modes that are unique for each pressure. In atmospheric pressure and room temperature conditions, dynamic measurements were obtained for the expected operational inflation pressure. Experimental mode shapes and frequency response functions for ambient conditions are described and compared to the results from the thermal vacuum tests. There is a surprising lack of correlation in test results between the two test conditions, which may be explained by damping and air mass considerations. Results of this investigation point out the necessity of testing inflatable space structures in vacuum conditions before they can be launched.**

## Introduction

INFLATABLE structures have been the subject of renewed interest in recent years for space applications such as communications antennas, solar thermal propulsion, and space solar power. A major advantage of using inflatable structures in space is their extremely light weight. This makes inflatables a perfect match for solar thermal propulsion because of the low thrust levels available. An obvious second advantage is on-orbit deployability and subsequent space savings in the launch configuration. A recent technology demonstrator flight for inflatable structures was the inflatable antenna experiment that was deployed in orbit from the Space Shuttle *Orbiter*. Although difficulty was encountered in the inflation/deployment phase, the flight was successful overall and provided valuable experience in the use of such structures.[1]

The solar orbital transfer vehicle, discussed in Ref. 2, is a planned technology demonstrator flight for solar thermal propulsion. The basic concept behind solar thermal propulsion is to utilize solar energy as a means of heating a working fluid (propellant) to provide thrust at increased specific impulse. As described in Ref. 3, thrust is produced by expanding the heated propellant through a nozzle. No combustion occurs, and the thrust level is low. For this reason, solar thermal propulsive systems are mainly applicable for orbital transfer vehicles.

Another technology demonstration program for solar thermal propulsion is the solar thermal upper stage (STUS), which is described in Refs. 4–6. The engine system envisioned for the STUS is designed to utilize hydrogen propellant to produce a thrust level of about 8.9 N (2 lb). Two inflatable parabolic collectors could be used that would be rotated and gimballed for focusing sunlight into an absorber cavity (Fig. 1; see Ref. 6). The collectors would be inflated after separation of the upper stage from the launch vehicle.

A number of other investigators have considered the use of inflatable structures for space applications. Perhaps the earliest was Otto,[7] who in 1962 published ideas for inflated tubular frames for use in structures such as orbiting platforms. A more recent proposed application involves the use of inflatable beam segments to replace solid segments of the space shuttle remote manipulator system and thus reduce storage space and inertia of the arm.[8]

Several papers on static structural analysis of inflated cylinders have been written, describing different techniques such as linear shell theory and nonlinear and variational methods.[9–17] Additional work of significance involves rigidization of inflated beam structures. One proposed concept is the use of injected foam that fills the cylindrical beam cross section, subsequently hardens, and, thus, rigidizes the structure. This approach is discussed in Ref. 18.

Very little work had been done in dynamics testing and analysis of inflatable structures until recent years. In 1988, Leonard[19] indicated that elastic beam bending modes could be utilized in approximating lower-order frequencies of inflatable beams. Main et al. wrote a very significant 1995 paper describing results of modal tests of inflated cantilever beams and the determination of effective material properties.[20] Changes in material properties for different pressures were also discussed, and the beam model was used in a more complex structure. The paper demonstrated that conventional finite element analysis packages could be very useful in the analysis of complex inflatable structures. Reference 21 describes an investigation of the dynamics of polyimide thin-film inflated cylinders, and Refs. 22–27 discuss recent dynamic tests and potential applications of inflatable solar concentrators.

## Description of Inflatable Solar Concentrator Investigated in the Current Study

In Fig. 2, a prototype inflatable solar concentrator is shown that consists of a torus/lens assembly supported by three struts. The torus has an inner diameter of 1.83 m (72 in.) and an outer diameter of 2.13 m (84 in.), with the 1.83-m (72-in.)-diam flexible Fresnel lens attached at the centerline of the inner diameter of the torus. Each strut is 1.85 m (73 in.) long with a uniform diameter of 0.10 m (4 in.). The concentrator is constructed of Kapton polyimide film, grade

Received 2 June 2000; revision received 25 August 2000; accepted for publication 1 September 2000. 

*Assistant Research Professor, Department of Mechanical Engineering and Materials Science, Edmund T. Pratt Jr. School of Engineering. Member AIAA.

†Aerospace Technologist, Structural Dynamics and Loads Group/ED21, Structures, Mechanics, and Thermal Department. Senior Member AIAA.

‡Aerospace Technologist, Structural Dynamics and Testing Group/ED27, Structures, Mechanics, and Thermal Department. Senior Member AIAA.

§Aerospace Technologist, Structural Dynamics and Testing Group/ED27, Structures, Mechanics, and Thermal Department. Member AIAA.

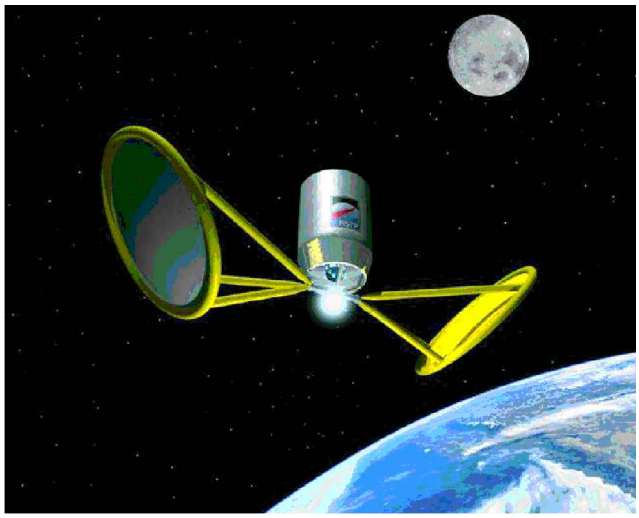

**Fig. 1 STUS concept.**

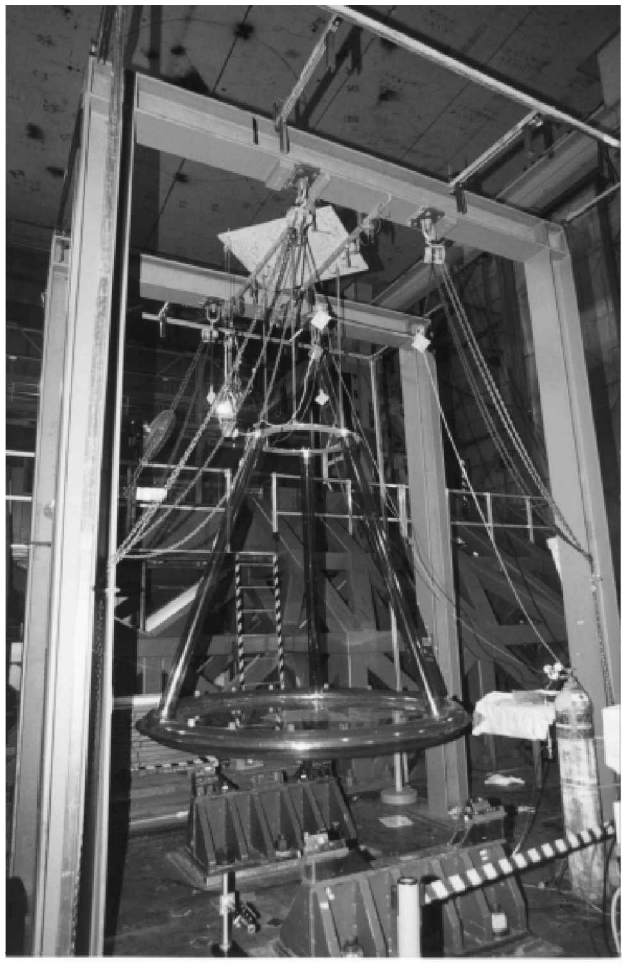

**Fig. 2 Pathfinder 3 inflatable test article.**

200HN for the struts, with a film thickness of 0.0051 cm (0.002-in.) and 300JP for the torus, which has a thickness of 0.0076 cm (0.003 in.). Epoxy is used as the primary adhesive for the joints. For the purposes of the prototype, the lens was simulated by a sheet of 0.0051-cm (2-in.) polyethylene film. In practical applications, the Fresnel lens or reflector of such a concentrator assembly would focus sunlight into a collector near the fixed ends of the struts. Solar energy stored in the collector could be utilized to heat a propellant as described earlier. The inflatable struts shown in Fig. 2 are attached to a base plate by means of three cylindrical appendages. These hollow appendages also allow inflation of the concentrator assembly through air hoses connected at each strut.

Inflatable structures are, in general, extremely lightweight, and the solar concentrator described in this paper is no exception. The thin-film inflatable portion of the concentrator, which enclosed a total volume of 0.158 $m^3$ (5.597 $ft^3$), was only 15% of the total mass of 9.75 kg (21.5 lb); the remaining mass was due to the aluminum interface plate and related hardware.

## Test Configurations and Results

### Modal Test Configuration and Procedures in Thermal Vacuum Conditions

Because of 1) current limitations in the accuracy of finite element models of inflatable structures and 2) lack of understanding of the behavior of inflatables in space, it was determined that the solar concentrator modal survey tests should be conducted in a thermal vacuum chamber. Such an approach allows testing in environments replicating orbital conditions as nearly as possible. Testing was done in NASA Marshall Space Flight Center's (MSFC) X-Ray Calibration Facility (XRCF). The facility includes a thermally controlled vacuum chamber 22.9 m (75 ft) long and 7.3 m (20 ft) in diameter, large enough to hold anything that will fit into the space shuttle's cargo bay. The vacuum chamber has both liquid nitrogen cooled panels and heater panels for simulating deep space operating conditions and for providing accurate thermal stability. Connecting the 500 m (1700 ft) between the x-ray sources and the instrument chamber is the guide tube. Thermal control range of the chamber is −107–71°C (−160–+160°F), and the lowest vacuum that can be obtained is $10^{-7}$ torr. Because of high flexibility of the polyimide film at any location on the inflated part of the concentrator that would have led to inadequate input power spectra, it was decided to utilize single-point random shaker excitation at a location on the interface plate (Fig. 2) as opposed to exciting the structure directly on the inflatable surface. Thus, random force input excitation was provided along the $X$ axis as defined in Fig. 3 by a Ling model V203 electrodynamic shaker attached to the interface plate by a phenolic stinger. The source signal to the shaker, provided by a Hewlett–Packard (HP) Model 35653C source module, was amplified by a Ling model TPO 25 amplifier. To remove the dc component of the random source signal and to prevent excitation of rigid-body modes, the source signal was high pass filtered at 0.5 Hz and low pass filtered at 100 Hz by a Wavetek model 852 filter before being amplified. Random force levels across all tests were approximately 0.08 N (0.018 lb) rms over the data acquisition bandwidth as measured by a PCB model 208B03 load cell.

The decision to provide excitation at the interface plate meant that the concentrator had to be suspended in a free–free boundary condition. A soft stainless steel spring system was designed to provide the lowest rigid-body frequencies possible and yet have the strength to suspend the test article above the floor of the vacuum chamber. Metal springs as opposed to soft rubber bungee cords were required for protection of the chamber interior.

Because any commercially available accelerometer, no matter how lightweight, would mass load the inflated components and the lens of the test article, a noncontacting vibration measuring device was needed. In addition, the limited number of cable feedthroughs in the thermal-vacuum chamber for accelerometers and that adhesives

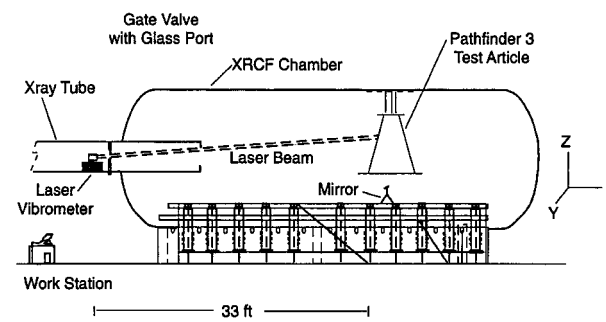


**Fig. 3 Diagram showing vibrometer location relative to test article in XRCF.**

could not be used in the chamber due to their outgassing characteristics further demonstrated the need for noncontact measurements. An Ometron VPI Sensor V/9100 scanning laser vibrometer was thus employed for this test, located relative to the test article and the vacuum chamber as shown in Fig. 3. The vibrometer output is acquired with an HP 3566/67 data acquisition system with an HP 3566 front end. The laser had to be aimed at the inflatable structure through a porthole at the end of the guide tube, which was the only location outside the chamber from which the test article could be viewed directly. For the vacuum test, 37 response points were measured on the torus and struts; no points on the lens were measured due the difficulty of measuring deflection in the $Z$ direction. The vibrometer measurement range used was for low velocities from 0.0 to 0.01 m/s. Calibration was achieved using a reference accelerometer. A discrete sinusoidal input is used in calibration for each decade and for each velocity setting of the vibrometer.

Response measurements on the surface of the inflatable concentrator were complicated by the polyimide material being optically transparent, allowing much of the laser light to pass through the test article, whereas the measurement method requires that laser light be reflected back to the sensor head. In addition, the laser beam should be as close to perpendicular as possible with respect to the test article surface to minimize any degradation in vibrometer measurements. This is true because the vibrometer is designed to measure the test article motion along the direction of the laser beam, and if the laser is not truly perpendicular to the surface, only a component of the real motion is measured. For the purposes of this series of tests, the cosine error that resulted from the location of the vibrometer at a single point for all measurements was considered to be negligible due to the distance from the vibrometer to the test article. All of these considerations required the use of surface treatments to facilitate testing. Sandblasted aluminum reflective tape was mounted at all points (struts and torus) where the measurements were to be taken. On the inflatable torus, the reflective tape was formed in the shape of corner cubes whose perpendicular sides were aligned with the $X$ and $Y$ axes. Mass loading due to the tape was minimal, with each corner cube having a mass of 0.04 g (0.0141 oz). Furthermore, the cubes do not have their own dynamics within the frequency range of interest in this test. The surface preparations are shown in Fig. 4.

Testing in the XRCF thermal vacuum chamber presented a number of difficulties, including limited accessibility to the test article for acquiring measurements. This limitation, along with the impracticality of suspending the test article from the side, prevented any measurements perpendicular to the plane of the torus/lens of the concentrator ($Z$ direction). Mode shapes could only be obtained for the $X$ and $Y$ directions, which were parallel to the plane of the torus/lens assembly.

Initially, the porthole direction was along the $X$ axis of the concentrator test article. Data were taken in this initial configuration at 21°C (70°F) for three inflation pressures of the concentrator relative to the chamber: 3447, 1724, and 5171 Pa (0.5, 0.25, and 0.75 psi), respectively, where 3447 Pa (0.5 psi) was the projected operating pressure for the flight article. Then the cryogenic portion of the test was conducted at a temperature of −48°C (−55°F) and concentrator inflation pressure relative to the chamber of 3447 Pa (0.5 psi). In the second testing configuration, the test article was rotated 90 deg such that the $Y$ axis was aligned with the porthole direction, whereas the shaker orientation was unchanged. These four test conditions were then repeated for the $Y$ direction.

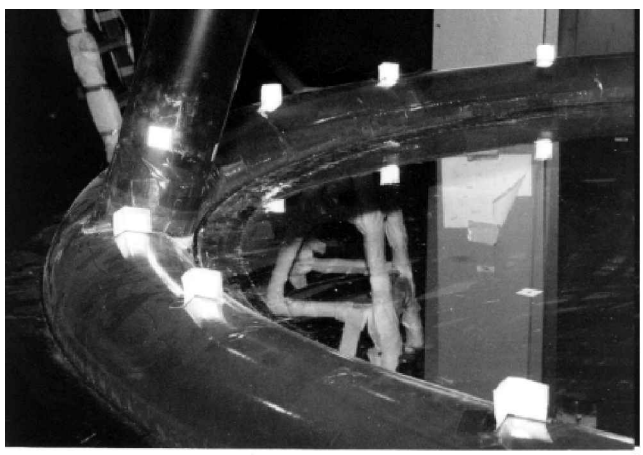

**Fig. 4 Surface preparations for use of vibrometer.**

### Discussion of Test Data for Thermal Vacuum Conditions

Modal parameters for all modes at frequencies under 50 Hz were successfully identified for the three pressures at 21°C test conditions using Spectral Dynamics STARStruct advanced curve fitter software. After mode indicator functions (MIF) and stability diagrams were produced, computational poles that indicated stability for greater than half of the model order and that corresponded with a dominant peak of the MIF were selected. The maximum available model order (30) was used. With their frequencies and damping, 12, 10, and 11 mode shapes were identified for the 3447, 1724, and 5171 Pa pressures, respectively. The modal properties for the nominal 21°C temperature conditions (Tables 1–3) showed characteristics seen in previous inflatable concentrators' modal tests done at MSFC, primarily the heavy ($\gg$1 %) damping of

**Table 1 Thermal vacuum modal frequencies and damping; 3447 Pa/21°C**

| Mode | Frequency, Hz | Damping, % |
|---|---|---|
| 1[a] | 0.836 | 15.68 |
| 2 | 3.71 | 4.76 |
| 3 | 5.66 | 3.51 |
| 4 | 11.00 | 1.29 |
| 5 | 13.79 | 0.98 |
| 6 | 26.77 | 0.46 |
| 7 | 27.70 | 1.88 |
| 8 | 34.39 | 0.85 |
| 9 | 35.84 | 2.18 |
| 10 | 39.40 | 2.41 |
| 11 | 41.62 | 0.90 |
| 12 | 43.79 | 1.23 |

[a]Test fixture suspension mode.

**Table 2 Thermal vacuum modal frequencies and damping; 1724 Pa/21°C**

| Mode | Frequency, Hz | Damping, % |
|---|---|---|
| 1[a] | 0.509 | 44.13 |
| 2 | 4.21 | 4.38 |
| 3 | 9.27 | 1.35 |
| 4 | 10.78 | 4.40 |
| 5 | 26.53 | 0.58 |
| 6 | 31.45 | 2.15 |
| 7 | 33.53 | 1.53 |
| 8 | 37.24 | 1.45 |
| 9 | 40.25 | 1.58 |
| 10 | 42.47 | 0.94 |

[a]Test fixture suspension mode.

**Table 3 Thermal vacuum modal frequencies and damping; 5171 Pa/21°C**

| Mode | Frequency, Hz | Damping, % |
|---|---|---|
| 1[a] | 0.847 | 18.87 |
| 2 | 3.81 | 5.07 |
| 3 | 5.80 | 2.08 |
| 4 | 13.16 | 1.96 |
| 5 | 26.86 | 0.71 |
| 6 | 34.72 | 0.86 |
| 7 | 36.55 | 2.68 |
| 8 | 39.67 | 2.01 |
| 9 | 42.12 | 1.17 |
| 10 | 44.58 | 0.87 |
| 11 | 46.68 | 0.93 |

[a]Test fixture suspension mode.

**Table 4 Thermal vacuum modal frequencies and damping; 3447 Pa/− 48°C**

| Mode | Frequency, Hz | Damping, % |
|---|---|---|
| 1 | 1.54 | 3.35 |
| 2 | 3.91 | 1.35 |
| 3 | 6.10 | 1.51 |
| 4 | 10.12 | 1.65 |
| 5 | 11.15 | 0.96 |
| 6 | 27.41 | 0.98 |
| 7 | 31.37 | 1.49 |
| 8 | 44.59 | 0.56 |

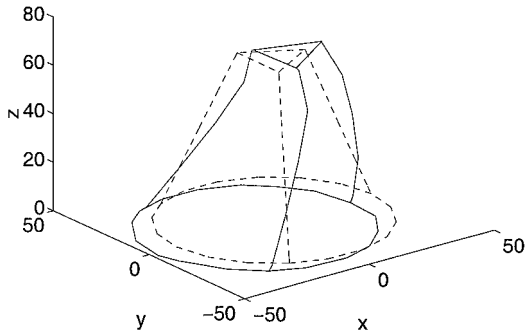


**Fig. 5 Third mode (5.66 Hz) of vacuum test case A (3447 Pa, 21°C).**

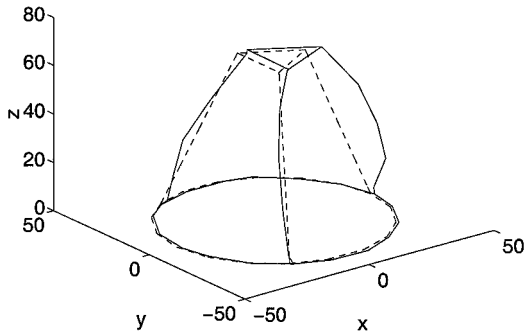


**Fig. 6 Seventh mode (27.70 Hz) of vacuum test case A (3447 Pa, 21°C).**

lower-order mode shapes. The cryogenic test case (3447 Pa, −48°C) yielded lower damping levels in the lower-order modes, as seen in Table 4. As expected from previous test experience,[21–24] modal frequencies increased slightly with increases in test article pressure. Inspection of mode shapes for each pressure configuration showed that some modes are very similar from one pressure to the next, but other modes are orphans, or unique for the pressure level. Some examples of these unique modes occurred at 13.79 and 39.40 Hz in the 3447-Pa (0.5 psi) test case. This observation points out the importance of carefully determining the operational on-orbit inflation pressure for the structure, as well as the need for testing in nonoperational conditions. Figures 5 and 6 show two typical mode shapes for the 3447-Pa, 21°C case, occurring at 5.66 Hz (third mode) and 27.70 Hz (seventh mode). The 5.66-Hz mode is notable in that it was the highest-amplitude peak in the frequency response function (FRF), and the 27.70-Hz mode is illustrative of the strut-dominated modes that occurred at higher frequencies.

The FRFs, which were generated using 20–30 averages, were less than optimal, exhibiting a noticeable amount of noise (closely spaced, low-amplitude peaks) between the major resonant peaks. This noise may be attributed to three problems or conditions. One is the possibility of inadequate force distribution through the concentrator. The high flexibility and high damping of the inflatable components may have hindered the propagation of energy through the structure from the interface plate. A second possible condition contributing to noisy FRFs may be the limitations of the shaker, where input power substantially decreased below 2 Hz. This caused an additional reduction in force input into the inflatable components in this frequency range. The third condition causing or contributing noise in the FRFs is the likelihood of local shell modes being present in the bandwidth of the global modes of the concentrator. These modes consist of small-amplitude radial oscillation of the inflatable elements resulting in wave patterns of expansion and contraction, which would result in behavior other than global bending being seen as noise in the FRFs. In general, the response functions showed the high damping and close modal coupling seen in the previous tests of inflatable concentrators.[23,24] Response function measurements during the low-temperature (−48°C) configuration were degraded primarily due to condensation on the porthole glass, but perhaps also due to changes in the polyimide film (increased brittleness at very low temperature) and possible loss of shaker performance. As a consequence, the cryogenic FRFs could not be used in the modal parameter identification process.

After the advanced curve fitter was used to obtain poles that were determined to represent resonant frequencies and their corresponding damping, mode shapes for each pole considered a resonant frequency were calculated using all of the FRFs that were measured. A least-squares fitting routine was used in calculating mode shape residues. A modal assurance criterion (MAC) matrix for each set of mode shapes was determined to verify the independence and orthogonality of the modes. The MAC is commonly used to determine the correlation between two modal vectors and is defined such that a set of independent normal modes would produce a MAC matrix having diagonal terms of 1.0 and off-diagonal terms of 0.0. Typically, off-diagonal terms of 0.1 or less are required to verify the independence of one mode from another and verify the quality of the measured mode shapes. However, due to 1) symmetry and nonlinearity of the structure, 2) highly damped and coupled mode shapes, 3) possible inadequate excitation to the structure, and 4) possible inadequate spatial resolution due to the limited number of measurement points, it was decided that any mode shape with an off diagonal of 0.4 or less would be considered an acceptable mode if it met certain conditions. These conditions were that the mode must 1) be global with respect to its deformations, 2) have a stable pole at low model orders with continued stability at higher model orders, and 3) have a distinctive peak in the MIF corresponding to the stable poles.[21–25] On the basis of comparisons between test data and model predictions, it was suspected that the suspension system coupled with the inflatable concentrator modes. Additional testing confirmed the coupling of the suspension system, and the springs had to be included in the model as accurately as possible. Such test-article-to-suspension coupling cannot be avoided in free–free tests of lightweight and highly flexible inflatable structures.

### Modal Survey Testing in Atmospheric Pressure

The purpose of testing the inflatable concentrator in a laboratory in atmospheric pressure and room temperature was twofold: 1) to compare dynamic characteristics of the structure in ambient and vacuum environments and 2) to provide measurements perpendicular to the plane of the torus/lens assembly ($Z$ direction), including the Fresnel lens simulator. Recall that the $Z$ measurements could not be obtained in the thermal vacuum chamber due to limitations on the laser vibrometer field of view and the impracticality of mounting the test article from the side.

Test article suspension configuration, strut and torus measurement point locations, and shaker location and orientation (for $X$ and $Y$ data) were the same as for the thermal vacuum tests. In addition to the 37 points on the struts and torus, 20 targets were placed on the lens, for a total of 57 measurement points. Of course, for the $Z$-direction measurements, the shaker was oriented in the $Z$ direction as well. The guiding purpose in this testing was to replicate as nearly as possible the test configuration utilized in the vacuum chamber, to make valid comparisons of the $X$- and $Y$-direction measurements. Visual checkout of the test article rigid-body modes on the suspension system revealed that vertical ($Z$ or plunge mode) and pendulum frequencies (both $X$ and $Y$ axes) were approximately 0.40 Hz. Obviously, this verifies the suspected coupling of the lowest frequency modes with the suspension system that was mentioned in the discussion of vacuum test results. This coupling was further verified at the beginning of the ambient testing by attaching lumped masses to the springs and observing changes in the frequency response. To

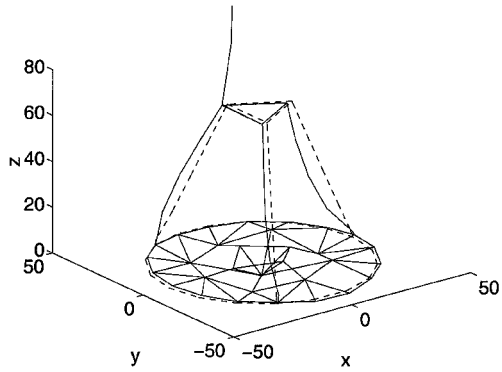


**Fig. 7 Ambient test strut-dominated mode, 24.73 Hz, *X*-axis excitation (mode 6).**

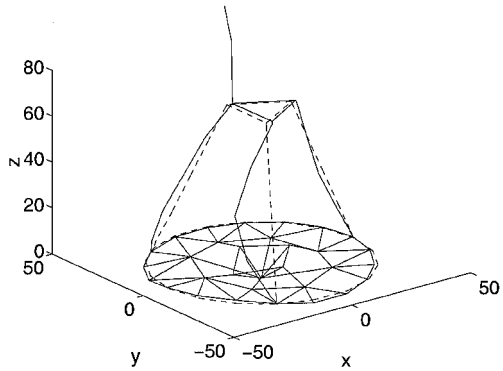


**Fig. 8 Ambient test strut-dominated mode, 24.58 Hz, *Z*-axis excitation (mode 7).**

better characterize the spring motion in the mode shapes, measurements points were added at four locations on one of the springs. Coupling of this nature is simply unavoidable in free–free testing of extremely lightweight and flexible inflatable (nonrigidized) structures. It appears that even with the best suspension system design, the flexibility of the test article will be on the same order as that of the suspension system.

As described earlier in the paper, the decision to do free–free testing was based on the difficulty of exciting the structure on the inflatable surface and the perceived necessity of providing excitation at the aluminum interface plate. The lesson learned in this approach, in light of the ever-present suspension coupling with the inflatable, is that constrained boundary conditions should be used in future testing and that the problem of exciting on the inflatable surface is less severe than the coupling problem.

Mode shapes and frequency response data were obtained for the $X$, $Y$, and $Z$ directions at 3447 Pa (0.5 psi) and approximately 21°C (70°F) average temperature. It was thought that atmospheric tests at only the operational inflation pressure would be sufficient for comparison to the vacuum environment. The test data are discussed in the next section.

#### Discussion of Test Results for the Atmospheric Pressure Environment

There were 10 modes identified for the $X$-axis shaker excitation configuration, and 12 modes were measured for the $Z$ excitation case. Going into the test, it was expected that many of the same modes would be excited in both shaker orientations. However, inspection of the modes revealed essentially two different sets. Strut-dominated modes appear in the frequency range above about 25 Hz in both cases, but even these modes are considerably different. Figures 7 and 8 show two such modes from the $X$ and $Z$ excitations, respectively. It is possible that the combined influences of the suspension system, with different stiffness characteristics and response in the $X$ and $Z$ directions, and shaker-imposed constraints are the cause of the lack of similarity between the $X$ and $Z$ excitation cases.

Tables 5 and 6 list the modal frequencies and damping for $X$ and $Z$ excitations, respectively. The clear observation to be made is that

**Table 5 Atmospheric modal frequencies and damping; 3447 Pa/21°C, *X* excitation**

| Mode | Frequency, Hz | Damping, % |
|---|---|---|
| 1 | 2.34 | 14.67 |
| 2 | 5.38 | 15.66 |
| 3 | 8.36 | 6.92 |
| 4 | 13.06 | 3.20 |
| 5 | 21.96 | 1.88 |
| 6 | 24.73 | 2.49 |
| 7 | 32.34 | 2.08 |
| 8 | 35.93 | 1.61 |
| 9 | 40.59 | 0.81 |
| 10 | 45.32 | 1.61 |

**Table 6 Atmospheric modal frequencies and damping; 3447 Pa/21°C, *Z* excitation**

| Mode | Frequency, Hz | Damping, % |
|---|---|---|
| 1 | 3.57 | 17.62 |
| 2 | 5.50 | 9.59 |
| 3 | 8.17 | 8.48 |
| 4 | 13.86 | 5.74 |
| 5 | 16.52 | 5.37 |
| 6 | 18.55 | 2.93 |
| 7 | 24.58 | 1.17 |
| 8 | 25.79 | 2.09 |
| 9 | 28.38 | 2.89 |
| 10 | 32.18 | 2.38 |
| 11 | 34.48 | 1.90 |
| 12 | 36.39 | 2.53 |

the first few modes in each case are very heavily damped, and, in fact, all of the modes have high damping. In general, this observation has been made in all dynamic testing of inflatable structures conducted at MSFC.

Additional observations of the modal properties in ambient conditions can be made related to the behavior of the torus and lens simulator. As described earlier in the paper, $Z$-direction measurements (direction perpendicular to the torus/lens plane) could not be made in the vacuum chamber. Several of the $X$-excitation modes, for example 13.06 and 21.96 Hz, show considerable out-of-plane bending of the torus. Also, most of the modes for both excitation cases have extensive $Z$-direction response of the lens simulator. These characteristics must be carefully considered in the design of inflatable structures for space flight, to achieve desired performance of the optical element.

Finally, MAC matrices were computed for the test modes in each of the $X$- and $Z$-excitation cases, to check their independence. In Table 7, the MAC matrix for the $X$-direction excitation is shown. It can be seen that the off-diagonal terms are high in several instances, such as 0.35 for 24.73 vs 13.06 Hz, and 0.41 for 5.38 vs 13.06 Hz. This is likely due to the symmetry of the structure and resulting similarity of some modes. Another contributing factor could be possible insufficient spatial resolution. Perhaps additional measurement points would improve the MAC. However, as stated in the discussion of vacuum-condition data, modes with high off-diagonal terms are still accepted as valid independent modes as long as the parameter identification conditions on global character and stability of poles at both low and high model orders are met.

## Comparison of Vacuum vs Atmospheric Test Results and Discussion of Differences

#### Frequency Response and Normal Modes

The normal modes of vibration for the vacuum and atmospheric conditions were compared numerically using the MAC, where the $X$–$Y$ projection of the ambient data with excitation in the $X$ direction was evaluated against the $X$–$Y$ measurements for the vacuum data. In comparing the measured solar concentrator modes in vacuum and ambient environments, only two modes were found to correlate with diagonal MAC values greater than 0.5. As seen in Table 8, which compares the eigenvectors from the 3447-Pa (0.5-psi) cases in vacuum and ambient with excitation in the $X$ direction and

**Table 7 MAC matrix, ambient vs ambient conditions; 3447 Pa, *X* excitation**

| Frequency, Hz | 2.34 | 5.38 | 8.36 | 13.06 | 21.96 | 24.73 | 32.34 | 35.93 | 40.59 | 45.32 |
|---|---|---|---|---|---|---|---|---|---|---|
| 2.34 | 1.00 | 0.01 | 0.10 | 0.08 | 0.04 | 0.13 | 0.00 | 0.02 | 0.01 | 0.00 |
| 5.38 | 0.01 | 1.00 | 0.18 | 0.41 | 0.33 | 0.29 | 0.01 | 0.03 | 0.01 | 0.02 |
| 8.36 | 0.10 | 0.18 | 1.00 | 0.08 | 0.15 | 0.16 | 0.00 | 0.00 | 0.02 | 0.11 |
| 13.06 | 0.08 | 0.41 | 0.08 | 1.00 | 0.26 | 0.35 | 0.00 | 0.01 | 0.00 | 0.04 |
| 21.96 | 0.04 | 0.33 | 0.15 | 0.26 | 1.00 | 0.19 | 0.01 | 0.08 | 0.01 | 0.03 |
| 24.73 | 0.13 | 0.29 | 0.16 | 0.35 | 0.19 | 1.00 | 0.12 | 0.31 | 0.07 | 0.00 |
| 32.34 | 0.00 | 0.01 | 0.00 | 0.00 | 0.01 | 0.12 | 1.00 | 0.08 | 0.17 | 0.04 |
| 35.93 | 0.02 | 0.03 | 0.00 | 0.01 | 0.08 | 0.31 | 0.08 | 1.00 | 0.27 | 0.27 |
| 40.59 | 0.01 | 0.01 | 0.02 | 0.00 | 0.01 | 0.07 | 0.17 | 0.27 | 1.00 | 0.05 |
| 45.32 | 0.00 | 0.02 | 0.11 | 0.04 | 0.03 | 0.00 | 0.04 | 0.27 | 0.05 | 1.00 |

**Table 8 MAC matrix, vacuum (rows) vs ambient (columns) conditions; 3447 Pa**

| Frequency, Hz | 3.71 | 5.66 | 11.00 | 13.79 | 26.77 | 27.70 | 34.39 | 35.84 | 39.40 | 41.62 |
|---|---|---|---|---|---|---|---|---|---|---|
| 2.34 | 0.00 | 0.00 | 0.11 | 0.00 | 0.00 | 0.02 | 0.00 | 0.06 | 0.00 | 0.00 |
| 5.38 | 0.07 | 0.83 | 0.22 | 0.45 | 0.00 | 0.02 | 0.00 | 0.03 | 0.01 | 0.00 |
| 8.36 | 0.07 | 0.24 | 0.05 | 0.26 | 0.00 | 0.10 | 0.01 | 0.17 | 0.00 | 0.00 |
| 13.06 | 0.04 | 0.64 | 0.23 | 0.51 | 0.00 | 0.09 | 0.03 | 0.09 | 0.01 | 0.00 |
| 21.96 | 0.03 | 0.48 | 0.00 | 0.15 | 0.02 | 0.02 | 0.00 | 0.03 | 0.00 | 0.00 |
| 24.73 | 0.04 | 0.33 | 0.01 | 0.15 | 0.05 | 0.17 | 0.11 | 0.11 | 0.16 | 0.00 |
| 32.34 | 0.00 | 0.00 | 0.17 | 0.11 | 0.01 | 0.01 | 0.02 | 0.00 | 0.08 | 0.11 |
| 35.93 | 0.01 | 0.02 | 0.06 | 0.00 | 0.08 | 0.08 | 0.07 | 0.03 | 0.21 | 0.02 |
| 40.59 | 0.00 | 0.00 | 0.23 | 0.12 | 0.00 | 0.00 | 0.00 | 0.00 | 0.10 | 0.02 |
| 45.32 | 0.00 | 0.00 | 0.28 | 0.22 | 0.01 | 0.00 | 0.00 | 0.03 | 0.08 | 0.01 |

**Table 9 Mode comparison for MAC >0.5 across structural pressure levels, vacuum test; 3447 and 1724 Pa**

| Frequency, Hz | | |
|---|---|---|
| 3447 Pa | 1724 Pa | MAC |
| 0.84 | —— | —— |
| 3.71 | —— | —— |
| 5.66 | 4.21 | 0.67 |
| 11.00 | 9.27 | 0.78 |
| 13.79 | —— | —— |
| 26.77 | 26.53 | 0.91 |
| 27.70 | —— | —— |
| 34.39 | 33.53 | 0.75 |
| 35.84 | —— | —— |
| 39.40 | —— | —— |
| 41.62 | 40.25 | 0.77 |
| 43.79 | 42.47 | 0.72 |

**Table 10 Mode comparison for MAC >0.5 across structural pressure levels, vacuum test; 3447 and 5171 Pa**

| Frequency, Hz | | |
|---|---|---|
| 3447 Pa | 5171 Pa | MAC |
| 0.84 | —— | —— |
| 3.71 | 3.81 | 0.93 |
| 5.66 | 5.81 | 0.94 |
| 11.00 | 13.16 | 0.75 |
| 13.79 | —— | —— |
| 26.77 | 26.86 | 0.98 |
| 27.70 | —— | —— |
| 34.39 | 34.72 | 0.98 |
| 35.84 | 36.55 | 0.63 |
| 39.40 | —— | —— |
| 41.62 | —— | —— |
| 43.79 | 44.58 | 0.84 |

measurement in the $X-Y$ plane, these modes were the 5.38/5.66-Hz mode and the 13.06/13.79-Hz mode.

Table 8 also shows a number of off-diagonal entries that are appreciably greater than zero, indicating a large degree of similarity between modes in an individual test case. This is borne out by the results of calculating the MAC matrix for the ambient test case against itself. Table 7 indicates that the nonzero off-diagonal terms are present even in this case. It is believed that the high off-diagonal terms result primarily from the symmetry of the structure, which results in a number of similar strut-dominated modes. Several such modes were observed, characterized by different combinations of strut bending. This leads to the conclusion that some of the experimentally determined normal modes of the structure in a given test case have enough similarity that they are not completely orthogonal. Tables 9 and 10 show that across differing pressurization levels in the vacuum test, some modes correlate very strongly and others do not.

Also, the FRFs for the test cases were compared. As may be expected by the previous results from the MAC calculations, the peaks that most closely corresponded occurred in the 5.7-Hz range and the 13.5-Hz range. Figures 9 and 10 show the results for vacuum testing across the three pressure levels, and Figs. 11 and 12 compare vacuum and ambient test results at 3447 Pa (0.5 psi) and 21°C (70°F). Note that the frequency response results for the strut and the torus have different vertical scales due to the difference in the magnitude of response. In Figs. 11 and 12, the solid line depicts the result in the vacuum test and the dashed line that of the ambient test. The marked difference in frequency peaks occurring in the higher frequency region is especially notable. Also note that there is not a significant vertical difference between the baseline in the vacuum test and the baseline in the ambient test. From this, it may be concluded that the differences in mass between the test cases caused by the presence of more or less air in the inflatable is not a major contributing factor to the differences in the FRFs.

**Damping**

Another comparison may be drawn from examining the results of calculation of modal damping ratios. Figures 13 and 14 show plots of damping vs frequency, where the + symbols indicate the ambient test and the ○ symbols the vacuum test. Figure 13 indicates the results for the 3447-Pa vacuum test and the ambient test and Fig. 14 the cryogenic vacuum test at a pressure of 3447 Pa and temperature of −48°C as compared to the ambient test at the same pressure and a temperature of 21°C (70°F). In these plots, it is seen that the ambient curves are shifted up and to the right from the vacuum

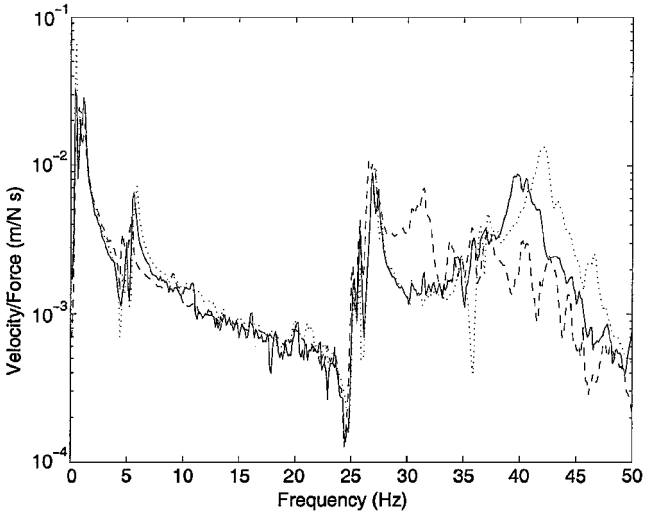


Fig. 9 Vacuum frequency responses across pressure levels for measurement point on strut: ——, 3447 Pa; – – –, 1724 Pa; and · · ·, 5171 Pa.

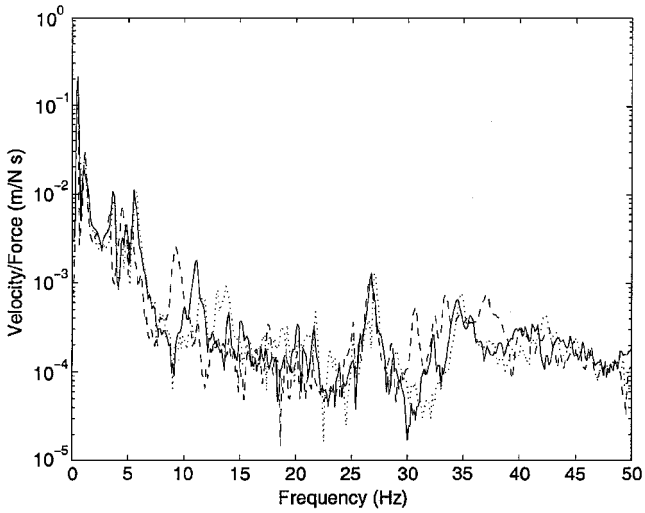


Fig. 10 Vacuum frequency responses across pressure levels for measurement point on torus: ——, 3447 Pa; – – –, 1724 Pa; and · · ·, 5171 Pa.

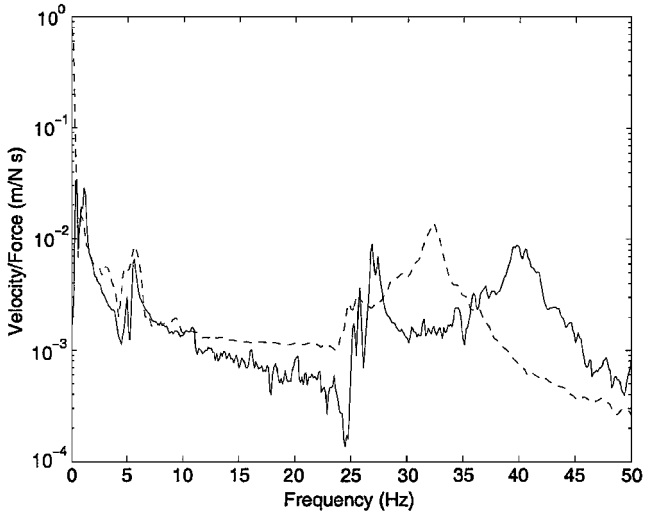


Fig. 11 Vacuum (——) vs ambient (– – –) FRFs for measurement point on strut, both at 3447 Pa.

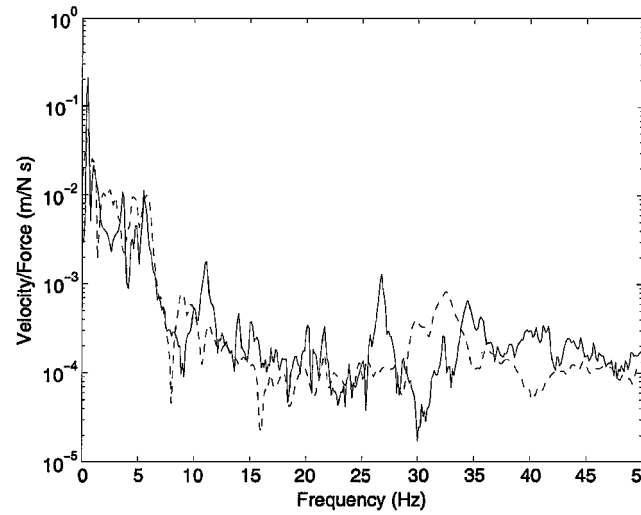


Fig. 12 Vacuum (——) vs ambient (– – –) FRFs for measurement point on torus, both at 3447 Pa.

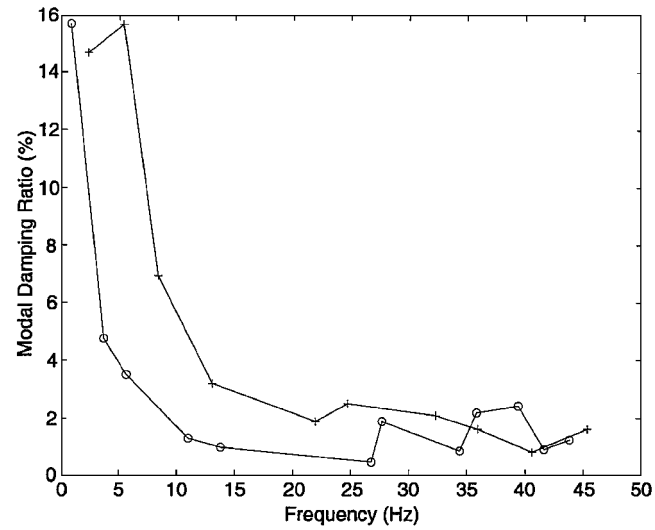


Fig. 13 Modal damping vs frequency for vacuum (∘) and ambient (+) conditions, both at 3447 Pa and 21°C.

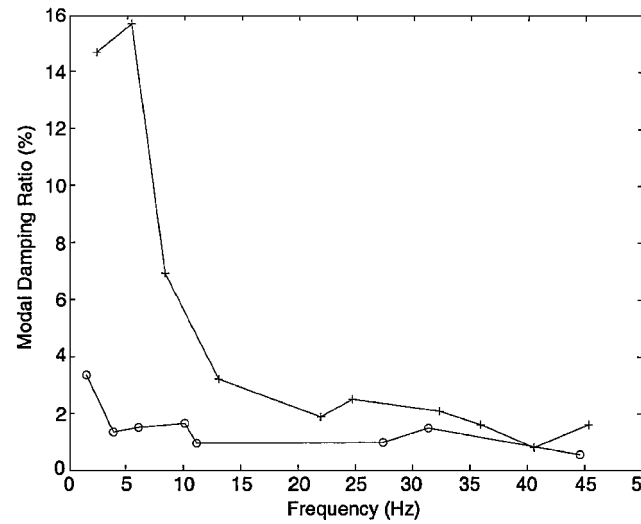


Fig. 14 Modal damping vs frequency for vacuum (3447 Pa, −48°C, ∘) and ambient (3447 Pa, 21°C, +) conditions.

curves, indicating a higher level of modal damping in the ambient cases. This is to be expected, because the ambient conditions provide damping in the form of air resistance, which the vacuum conditions remove. Also note that in the cryogenic test, shown in Fig. 14, the damping level is lower than that of the other vacuum tests.

## Summary

Modal testing was conducted on the Pathfinder 3 inflatable structure for the shooting star experiment. Tests were conducted under ambient laboratory conditions and in thermal vacuum, both at room temperature and in cryogenic conditions. The test results, and analysis of the results, indicate that there are significant differences between the performance of the structure in ambient and vacuum conditions. MAC calculations showed good correspondence between ambient and vacuum for only two modes, and the other modes were not well correlated. Comparison of FRFs confirmed these correlations. Also, the damping levels found in the ambient test were higher than those of the vacuum test. The results of this study point to a need to conduct vacuum modal surveys of inflatable articles intended for space applications to ensure that on-orbit behavior will be well replicated in the test environment.

## References

[1]Freeland, R. E., "Inflatable Antenna Flight Experiment Experiences," *NASA Solar Thermal Propulsion Workshop Proceedings*, NASA Marshall Space Flight Center, 1997.

[2]Partch, R., "Solar Thermal Propulsion Program at Phillips Lab," *NASA Solar Thermal Propulsion Workshop Proceedings*, NASA Marshall Space Flight Center, 1997.

[3]Stewart, J. F., and Martin, J. A., "Dual Fuel Solar Thermal Stage: Ideal Analysis," *Journal of Spacecraft and Rockets*, Vol. 33, No. 5, 1996, pp. 752–754.

[4]Patel, S., and Emrich, W. J., Jr., "Solar Thermal Upper Stage (STUS) Feasibility Study," *Proceedings of ASME/JSME/JSES International Solar Energy Conference*, American Society of Mechanical Engineers, 1995, pp. 809–816.

[5]Hawk, C. W., and Adams, A. M., "Conceptual Design of a Solar Thermal Upper Stage (STUS) Flight Experiment," AIAA Paper 95-2842, 1995.

[6]Curtis, L., "NASA Solar Thermal Propulsion Project," *NASA Solar Thermal Propulsion Workshop Proceedings*, NASA Marshall Space Flight Center, 1997.

[7]Otto, F., *Tensile Structures*, Massachusetts Inst. of Technology, Cambridge, MA, 1962.

[8]McCarty, L. H., "Inflatable Arm Segments May Lighten Shuttle's Manipulator System," *Design News*, Vol. 46, No. 4, 1990, pp. 150, 151.

[9]Leonard, R. W., Brooks, G. W., and McComb, H. G., Jr., "Structural Considerations of Inflatable Reentry Vehicles," NASA TN D-457, 1960.

[10]Topping, A. D., "Shear Deflections and Buckling Characteristics of Inflated Members," *Journal of Aircraft*, Vol. 1, No. 5, 1964, pp. 289–293.

[11]Bulson, P. S., "Design Principles of Pneumatic Structures," *Structural Engineering*, Vol. 51, No. 6, 1973, pp. 209–215.

[12]Douglas, W. J., "Bending Stiffness of an Inflated Cylindrical Cantilever Beam," *AIAA Journal*, Vol. 7, No. 7, 1969, pp. 1248–1253.

[13]Steeves, E. C., "A Linear Analysis of the Deformation of Pressure Stabilized Tubes," U.S. Army Natick Labs., Rept. AD/A-006 493, 1975; also National Technical Information Service, N75-32513, 1975.

[14]Fichter, W. B., "A Theory for Inflated Thin-Wall Cylindrical Beams," NASA TN D-3466, June 1966.

[15]Comer, R. L., and Levy, S., "Deflections of an Inflated Circular-Cylinder Cantilever Beam," *AIAA Journal*, Vol. 1, No. 7, 1963, pp. 1652–1655.

[16]Webber, J. P. H., "Deflections of Inflated Cylindrical Cantilever Beams Subjected to Bending and Torsion," *Aeronautical Journal*, Vol. 86, No. 858, 1982, pp. 306–312.

[17]Main, J. A., Peterson, S. W., and Strauss, A. M., "Load-Deflection Behavior of Space-Based Inflatable Fabric Beams," *Journal of Aerospace Engineering*, Vol. 7, No. 4, 1994, pp. 225–238.

[18]Hobbs, K. P., Jr., Smith, S. W., and Main., J. A., "Postflight Testing and Analysis of Zero-G Foam Rigidized Struts," *Proceedings of the 40th Structures, Structural Dynamics, and Materials Conference*, AIAA, Reston, VA, 1999.

[19]Leonard, J. W., *Tension Structures*, McGraw–Hill, New York, 1988.

[20]Main, J. A., Carlin, R. A., Garcia, E., Peterson, S. W., and Strauss, A. M., "Dynamic Analysis of Space-Based Inflated Beam Structures," *Journal of the Acoustical Society of America*, Vol. 97, No. 2, 1995, pp. 1035–1045.

[21]Slade, K. N., and Tinker, M. L., "Analytical and Experimental Investigation of the Dynamics of Polyimide Inflatable Cylinders," AIAA Paper 99-1518, 1999.

[22]Tinker, M. L., "Passively Adaptive Inflatable Structure for the Shooting Star Experiment," AIAA Paper 98-1986, 1998.

[23]Lassiter, J., "Shooting Star Experiment Prototype Inflatable Strut/Torus Assembly Modal Survey," NASA Test Rept. ED73(97-69), June 1997.

[24]Engberg, R., and Lassiter, J., "Shooting Star Experiment, Pathfinder 2, Inflatable Concentrator Modal Survey in Vacuum Conditions," NASA Test Rept. SSE-DEV-ED97-120, March 1998.

[25]Engberg, R., and Lassiter, J., "Shooting Star Experiment, Pathfinder 3, Inflatable Concentrator Modal Survey in Thermal-Vacuum Conditions," NASA Test Rept. SSE-DEV-ED97-115, Feb. 1998.

[26]Engberg, R., and Lassiter, J., "Shooting Star Experiment, Pathfinder 3, Inflatable Concentrator Terminator Test," NASA Test Rept. SSE-DEV-ED98-046, July 1998.

[27]Lassiter, J., and Engberg, R., "Dynamic Testing of an Inflatable Structure Under Thermal-Vacuum Conditions," AIAA Paper 99-1519, 1999.

A. Berman
*Associate Editor*